Time-shifting correction in optoacoustic tomographic imaging for media with non-uniform speed of sound

X Luís Deán-Ben, Vasilis Ntziachristos and Daniel Razansky*

Institute for Biological and Medical Imaging, Technical University of Munich and Helmholtz Center Munich, Ingolstädter Landstraße 1, 85764 Neuherberg, Germany.

ABSTRACT

An analysis of the time-shifting correction in optoacoustic tomographic reconstructions for media with an *a priori* known speed of sound distribution is presented. We describe a modification of the filtered back-projection algorithm, for which the absorbed optical energy at a given point is estimated from the value of the measured signals at the instant corresponding to the time-of-flight between such point and the measuring points. In the case that a non-uniform speed of sound distribution does exist, we estimate the time-of-flight with the straight acoustic rays model, for which acoustic waves are assumed not to change direction as they propagate. The validity of this model is analysed for small speed of sound variations by comparing the predicted values of the time-of-flight with the ones estimated considering the refraction of the waves. Experimental results with tissue-mimicking agar phantoms with a higher speed of sound than water showcase the effects of the time-shifting of the optoacoustic signals caused by the acoustic mismatch. The performance of the time-shifting correction relates to the optoacoustic imaging of biological tissues, for which the speed of sound variations are usually lower than 10%.

Keywords: Optoacoustic tomography, back-projection algorithm, heterogeneous speed of sound

1. INTRODUCTION

Optoacoustic tomography (OAT) is an emerging non-invasive biomedical imaging technique with applications in anatomical, functional and molecular imaging.[1–3] OAT presents important advantages derived from the synergetic combination of optics and ultrasound into a single modality. In particular, the technique exploits the contrast generated by optical absorption mechanisms and the ultrasonic detection principles to image biological tissues with high contrast and high resolution for depths in the order of several millimetres to centimetres.[4]

In OAT, the sample is usually illuminated with a short-pulsed laser verifying thermal confinement conditions.[5] Thereby, the absorption of light causes a pressure distribution at the initial instant that originates high frequency ultrasonic waves, which are then detected at different positions around the imaged object. Image reconstruction in OAT consists in the calculation of the initial pressure (which is proportional to the optical absorbed energy) from the measured pressure. For this, several algorithms have been reported in which a uniform speed of sound is commonly assumed. Among them, back-projection algorithms are frequently employed due to their ease of implementation and fast computational time.[6,7] In these algorithms, the absorbed optical energy is obtained by projecting the value of a quantity depending on the measured signal at a given instant back to the points in which the wave may have been excited to reach the transducer at such instant. Thereby, the reconstructed image is rendered by adding up the contributions from all the positions of the transducer.

In practical cases, regions with varying acoustic impedance may exist and distorted images may be obtained if a homogeneous acoustic medium with uniform speed of sound is assumed to make the reconstruction.[8–11] A non-constant speed of sound affects the time-of-flight of the ultrasonic waves from the excitation point until the position of the transducer, in a way that the reconstruction algorithms must be modified accordingly to avoid unwanted effects in the reconstructed images. For example, the curves along which the back-projection for a given instant is done in the back-projection algorithms can be changed taking into account the time-of-flight alterations. In general, the speed of sound variations in different biological tissues are rarely higher than

*E-mail: dr@tum.de

Novel Biophotonic Techniques and Applications, edited by Henricus J. C. M. Sterenborg, I. Alex Vitkin, Proc. of SPIE-OSA Biomedical Optics, SPIE Vol. 8090, 809013 · © 2011 SPIE-OSA · CCC code: 1605-7422/11/$18 · doi: 10.1117/12.889946

10%.[12] For such small variations of the speed of sound, the refraction or bending of the acoustic waves is usually neglected, so that the propagation of the waves is modelled as straight acoustic rays and the main effect of the speed of sound variations is a time-shifting of the optoacoustic signals.[8] Then, the time-of-flight is approximated as the integral of the inverse of the speed of sound along a straight line between the excitation and measuring points.

In this work, we analyse the effect of the time-shifting correction in optoacoustic tomographic reconstructions for media with an *a priori* known speed of sound distribution. Specifically, we analyse the case in which a circular region with a different speed of sound than the background does exist. The validity of the straight acoustic rays model for the estimation of the time-of-flight is analysed. For this, we compare the time-of-flight obtained by using such model with the time-of-flight obtained by considering the refraction of the waves. A modification of the filtered back-projection algorithm that takes into account the time-of-flight calculated from the *a priori* known speed of sound distribution is introduced. It is tested experimentally by imaging tissue-mimicking phantoms having a speed of sound approximately 10% higher than water. The presented results allow concluding on the feasibility of implementing the correction of the effects caused by small variations in the speed of sound in optoacoustic reconstruction algorithms, which relates to the performance of such correction for optoacoustic imaging of biological tissues.

2. THEORY

2.1 Straight acoustic rays model

The time-of-flight (TOF) corresponding to the propagation of a wave from a point P_1 until a point P_2 is given as the integral of the inverse of the speed of sound along the path of propagation l_{12}, i.e.,

$$T_{12} = \int_{l_{12}} \frac{1}{c}\, dl \tag{1}$$

For small variations in the speed of sound, the TOF can be estimated by using the straight acoustic rays model (SARM), in which the wave is assumed not to change direction as it propagates. Thereby, the path l_{12} in Eq. 1 is taken as a straight line.

A more accurate model for the propagation of the waves consists in considering the Fermat's principle, which states that the path of the acoustic rays is the one that corresponds to the least propagation time. In such case, l_{12} in Eq. 1 is taken accordingly. The Fermat's principle can be applied to model the refraction of the waves in the interface of two media with speeds of sound c_1 and c_2 respectively. In such case, the refracted angle θ_r is estimated from the incident angle θ_i (Fig. 1) according to the Snell's law as

$$\theta_r = \arcsin\left(\frac{c_2}{c_1}\sin\theta_i\right) \tag{2}$$

The wavefronts corresponding to a wave propagating along the interface between two media, i.e., the set of points having the same time delay, can be estimated by means of the Snell's law. For example, for a plane wave traversing a plane interface (Fig. 1), the transmitted wavefront $\mathrm{C}-\mathrm{D}$ is estimated from the incident wavefront $\mathrm{A}-\mathrm{B}$ by taking into account the refraction of the wave, so that the transmitted wavefront forms an angle θ_r (Eq. 2) with the interface of the two media. If the SARM is used, a transmitted wavefront $\mathrm{C}-\mathrm{D}'$ is estimated, which forms an angle θ_{AR} with the interface given by (Appendix A)

$$\theta_{AR} = \arctan\left(\frac{c_2\sin\theta_i\cos\theta_i}{c_1 - c_2\sin^2\theta_i}\right) \tag{3}$$

As mentioned above, the speed of sound variations in different biological tissues are normally confined in the range ±10% with respect to the speed of sound in water. Fig. 2 shows a comparison of θ_r and θ_{AR} as a function of θ_i for the case of an interface water-tissue with a ±10% difference in the speed of sound. For this, we considered a speed of sound in water $c_w = 1500$ m/s and speeds of sound in tissue of $c_t = 1350$ m/s and $c_t = 1650$ m/s respectively. It is shown that the angles θ_r and θ_{AR} are very similar except for the case of high values of θ_i. This appears to indicate the convenience of the SARM for estimating the transmitted wavefront, i.e., the set of points corresponding to a given TOF from the points of the incident wavefront.

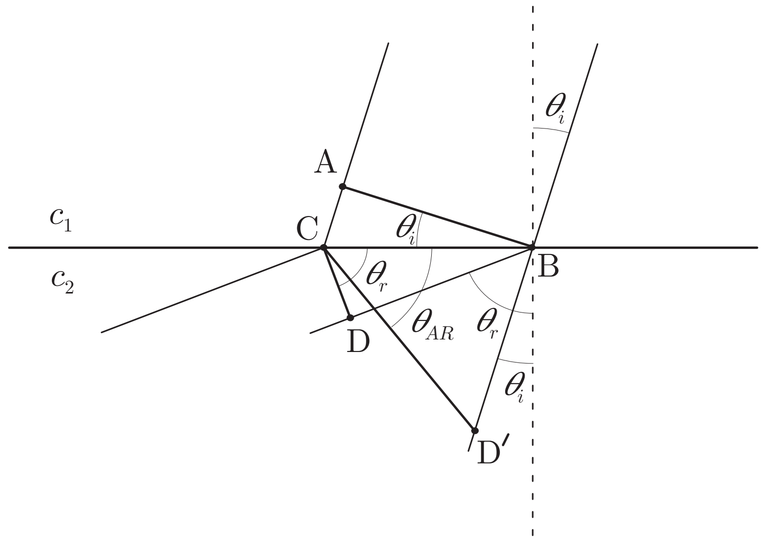

Figure 1. Transmission of a plane wave through the interface of two media with different speeds of sound as modelled by the Snell's law and by the straight acoustic rays model.

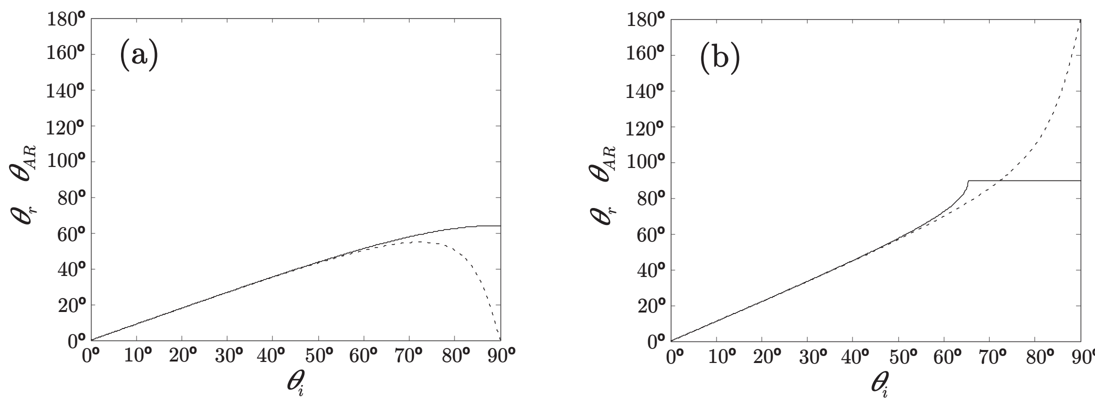

Figure 2. Angle of the transmitted wavefront as a function of the incident angle θ_i for a plane wave traversing a plane interface. The continuous lines indicate the angle predicted by the Snell's law θ_r and the dashed lines indicate the angle predicted by the straight acoustic rays model θ_{AR}. The first medium is water with speed of sound $c_w = 1500$ m/s and the second medium is biological tissue with $c_t = 1350$ m/s (a) or $c_t = 1650$ m/s (b).

2.2 Filtered back-projection algorithm in media with non-uniform speed of sound

For a homogeneous acoustic medium illuminated with pulsed-laser radiation, the thermal diffusion can usually be neglected and the temporal profile of the optical absorbed energy at any point can be approximated by a Dirac delta $\delta(t)$. Under these conditions, the pressure field $p(\boldsymbol{r}, t)$ corresponding to the generated ultrasonic wave satisfies

$$\frac{\partial^2 p(\boldsymbol{r}, t)}{\partial t^2} - c^2 \nabla^2 p(\boldsymbol{r}, t) = \Gamma H(\boldsymbol{r}) \frac{\partial \delta(t)}{\partial t} \tag{4}$$

where c is the speed of sound in the medium and Γ is the Grueneisen parameter (dimensionless). $H(\boldsymbol{r})$ is the optical absorption field, i.e., the amount of energy absorbed in the tissue per unit volume. Eq. 4 can be solved analitically resulting in the Poisson's solution for the pressure field given by

$$p(\boldsymbol{r}, t) = \frac{\Gamma}{4\pi c} \frac{\partial}{\partial t} \int_{S'} \frac{H(\boldsymbol{r}')}{|\boldsymbol{r} - \boldsymbol{r}'|} dS' \tag{5}$$

being S' a time-dependent spherical surface for which $|\boldsymbol{r}-\boldsymbol{r}'|=ct$. Eq. 5 establishes that the pressure $p(\boldsymbol{r},t)$ in a homogeneous acoustic medium is solely due to the optical absorption at locations $\boldsymbol{r}'$ so that the generated waves require time t to reach $\boldsymbol{r}$.

The filtered back-projection (FBP) algorithm can be used to estimate the optical absorption field $H(\boldsymbol{r}')$ from the pressure on a surface S enclosing $\boldsymbol{r}'$ as[7]

$$H(\boldsymbol{r}')=\frac{1}{\Gamma}\int_{\Omega}\frac{d\Omega}{\Omega}\left[2p(\boldsymbol{r},t)-2t\frac{\partial p(\boldsymbol{r},t)}{\partial t}\right]\Bigg|_{t=|\boldsymbol{r}-\boldsymbol{r}'|/c} \tag{6}$$

According to Eq. 6, the reconstruction consists in projecting the value of the quantity $2p(\boldsymbol{r},t)-2t\partial p(\boldsymbol{r},t)/\partial t$ for a given instant t and for a given point $\boldsymbol{r}$ back onto the spherical surface where a wave should be generated to reach the point $\boldsymbol{r}$ at instant t as indicated by Eq. 5. Equivalently, we can consider that the aforementioned quantity for an instant t is projected onto the wavefront corresponding to an impulse-type wave generated at $\boldsymbol{r}$ at $t=0$.

In some practical situations, for instance when the signals are collected with a cylindrically focused ultrasonic transducer scanned along a circumference surrounding the imaged object, it is acceptable to assume that all the optoacoustic sources lie in the imaging plane, which corresponds to a two-dimensional reconstruction. In this case, an approximate back-projection solution for the circular-scan geometry can be considered.[6] Furthermore, if the scanning radius is much larger than the size of the object, the solid angle $d\Omega$ in Eq. 6 for a given surface element dS (Eq. 6) is approximately constant for any position along the scanning circumference. Under these conditions, a 2D discretization of Eq. 6, in which for simplicity all the constants are dropped, is given by

$$H\left(\boldsymbol{r}'_j\right)=\sum_i\left[p\left(\boldsymbol{r}_i,t_{ij}\right)-t_{ij}\frac{\partial p\left(\boldsymbol{r}_i,t_{ij}\right)}{\partial t}\right] \tag{7}$$

where $\boldsymbol{r}_i$ is the position of i-th transducer, $\boldsymbol{r}'_j$ is the position of the j-th point of the reconstruction region of interest and $t_{ij}=|\boldsymbol{r}_i-\boldsymbol{r}'_j|/c$.

In media with a space-dependent speed of sound, Eq. 7 may not be a valid approximation so that distorted images may be obtained. In that case, we can modify Eq. 7 considering that for a given transducer i the back-projection is done onto the wavefronts corresponding to an impulse-type wave generated at $\boldsymbol{r}_i$ at $t=0$. Thereby, t_{ij} corresponds to the TOF from $\boldsymbol{r}_i$ until $\boldsymbol{r}'_j$, i.e.,

$$t_{ij}=\int_{l_{ij}}\frac{1}{c(\boldsymbol{r})}\,dl \tag{8}$$

In order to perform the optoacoustic reconstruction by means of Eqs. 7 and 8, the spatial distribution of the speed of sound must be known *a priori*. It can be measured by pure ultrasonic techniques such as ultrasonic transmission tomography[13] or by a optoacoustically-based system integrated in the imaging set-up.[14] In practice, a discretization of Eq. 8 must be used. For example, by applying a trapezoidal approximation of the integral t_{ij} can be estimated as

$$t_{ij}=\frac{1}{2}\sum_k\left(\frac{1}{c_k}+\frac{1}{c_{k+1}}\right)|\boldsymbol{r}_k-\boldsymbol{r}_{k+1}|, \tag{9}$$

being $\boldsymbol{r}_k$, with $k=1,2,...,N$, the positions of a set of N points along the path of propagation of the wave.

2.3 Loss of resolution due to errors in the time-of-flight

A wrong estimation of the TOF between the position of the transducers and the grid of points for which the reconstruction is made leads to a distortion in the recontructed image obtained with the FBP algorithm. Such distortion limits the maximum achievable resolution. To understand this we can consider an easy example in which the signal corresponding to a point source is acquired along a circumference of radius R (Fig. 3). We assume that the space-dependent speed of sound $c(\boldsymbol{r})$ presents small variations with respect to the speed of

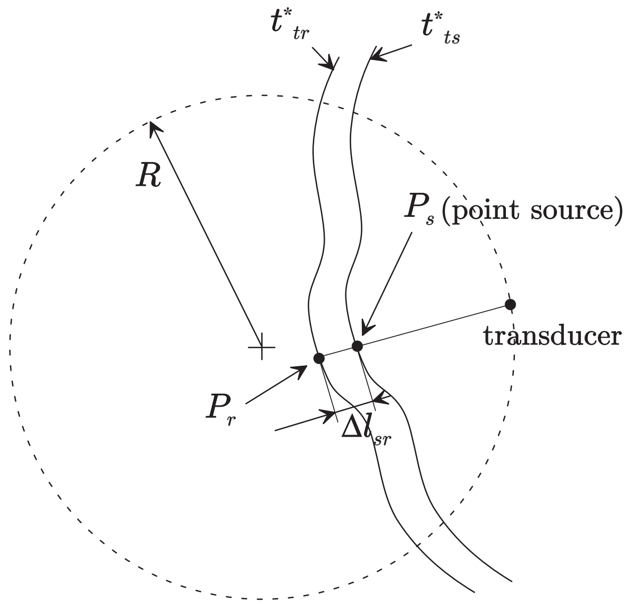

Figure 3. Error in the tomographic reconstruction due to a wrong estimation of the time-of-flight.

sound in water c_w, as in the case of most biological tissues. Let us assume that the actual TOF from the position of the transducer P_t until the position of the source P_s (Fig. 3) is equal to t_{ts}, i.e.,

$$t_{ts} = \int_{l_{ts}} \frac{1}{c\,(\boldsymbol{r})}\, dl, \tag{10}$$

i.e., the impulse-type signal originated at the source at $t = 0$ is measured with the transducer at $t = t_{ts}$. If a uniform speed of sound equal to the speed of sound in water is assumed, the estimated TOF t^*_{ts} from P_t until P_s is given by

$$t^*_{ts} = \int_{l_{ts}} \frac{1}{c_w}\, dl = \frac{l_{ts}}{c_w}, \tag{11}$$

so that the error in the TOF $|\Delta t_{ts}|$ due to a wrong assumption of the speed of sound is given by

$$|\Delta t_{ts}| = |t_{ts} - t^*_{ts}|. \tag{12}$$

For a given point P_r, it is verified that the estimated TOF t^*_{tr} from P_t until P_r is equal to the actual TOF t_{ts}, i.e.,

$$t^*_{tr} = \frac{l_{tr}}{c_w} = t_{ts}. \tag{13}$$

Then,

$$|\Delta t_{ts}| = \left|\frac{l_{tr}}{c_w} - \frac{l_{ts}}{c_w}\right| = \left|\frac{l_{rs}}{c_w}\right|. \tag{14}$$

The wrong assumption of the speed of sound leads to considering that the signal measured at P_t at t_{ts} was originated at the points of the curve for which the estimated TOF $t^* = t^*_{tr}$ (Fig. 3), which leads to a distortion in the reconstructed image. The error in the location of an optoacoustic source Δx is in the order of

$$|\Delta x| \approx |l_{sr}| = c_w |\Delta t_{ts}|. \tag{15}$$

3. NUMERICAL SIMULATION

In section 2.1 it was shown that the curves corresponding to a given TOF predicted by the SARM are very similar to the actual ones for the case of a plane wave traversing a plane interface. In this section, we perform numerical simulations to estimate the shape of such curves for the case in which a circular region with a 10% higher speed of sound than the background does exist. For this, we considered a grid of 50×50 equally spaced points covering a 20×20 mm^2 region of interest (ROI), so that the pixel size is $\Delta xy = 400$ μm. We considered that the transducer is located 40 mm away from the centre of the ROI. We assumed a background speed of sound $c_1 = 1500$ m/s, so that the speed of sound inside the mismatch region is taken as $c_2 = 1650$ m/s.

First, we compared the TOF for the points of the grid calculated with Eq. 1 by considering that l_{12} is a straigth line according to the SARM or a set of segments verifying Snell's law. The estimated curves for a constant TOF are depicted in Fig. 4a for circular mismatched region with a radius $R_{\mathrm{s}} = 6$ mm. The continuous blue lines represent the curves obtained with the SARM and the dashed red lines stand for the curves obtained by considering the refractions of the wave. It is shown that the resulting curves obtained with both models are very similar, especially within the mismatch region. In order to quantify the difference between the results obtained with both models, we computed the root mean square difference Δt of the TOF predicted by both models for the points of the grid. The results are shown in Fig. 4b as a function of R_{s}.

In a second step, we compared the TOF predicted by the SARM for the points of the grid by considering the continuous integral of Eq. 8 and the discrete approximation of Eq. 9. The estimated curves for a mismatch region with a radius $R_{\mathrm{s}} = 6$ mm are shown in Fig. 4c, where the discrete integral was calculated by considering a step of $5\Delta xy$. We also calculated the root mean square difference of the TOF predicted by the continuous and discrete integrals. The results are shown in Fig. 4d as a function of R_{s} and the integration step. It is shown that the error in the estimation of the TOF due to the discretization of the integral is in some cases comparable to the intrinsic error of the SARM, and can even be dominant if the integration step is not fine enough. In any case, the curves along which the back-projection is done are very similar in all cases. Then, in principle, it is feasible to do the correction by considering a discrete approximation of the integral.

4. EXPERIMENT

The correction of time-shifting effects in tomographic reconstructions was tested experimentally by imaging tissue-mimicking agar phantoms in which glycerine was included to simulate a higher speed of sound than water.

4.1 Experimental set-up

The experimental setup consisted of an optical parametric oscillator (OPO)-based laser (MOPO series, Spectra Physics), pumped by a nanosecond pulsed Nd:YAG laser (Lab-190-30, Spectra-Physics) with 15 Hz pulse repetition, which is used as the illuminating source at a wavelength of 605 nm. The output laser beam was shaped in order to achieve ring-type uniform illumination conditions on the surface of the phantom. A cylindrically-focused ultrasonic immersion PZT transducer (model V382, Panametrics-NDT, Waltam, MA) with a center frequency of 3.5 MHz and a focal length of 38.1 mm was used to collect the time-resolved signals, which are then band-pass filtered with cutoff frequencies of 0.1 and 5 MHz. The sample is rotated with a high speed rotation stage (Thorlabs PRM1/M-Z7) with angular steps of 2° along a whole circumference, so that 180 tomographic projections are acquired. More details on the experimental setup can be found elsewhere.[15]

4.2 Phantoms

Several tissue-mimicking phantoms were used in the experiment. They were made with a mixture of agar solution (66% by volume) and glycerine (33% by volume) in which black India ink and Intralipid were added in order to simulate the tissue background optical absorption and background optical scattering respectively. In particular, we added 0.002% by volume of ink and 1.2% by volume of Intralipid, which correspond, respectively, to an optical absorption coefficient $\mu_{\mathrm{a}} = 0.2$ cm^{-1} and to a reduced scattering coefficient of $\mu_{\mathrm{s}}' = 10$ cm^{-1}. Regions with higher optical absorption were added, in which the concentration of black ink is 0.01% by volume, corresponding to an optical absorption coefficient $\mu_{\mathrm{a}} = 1$ cm^{-1}.

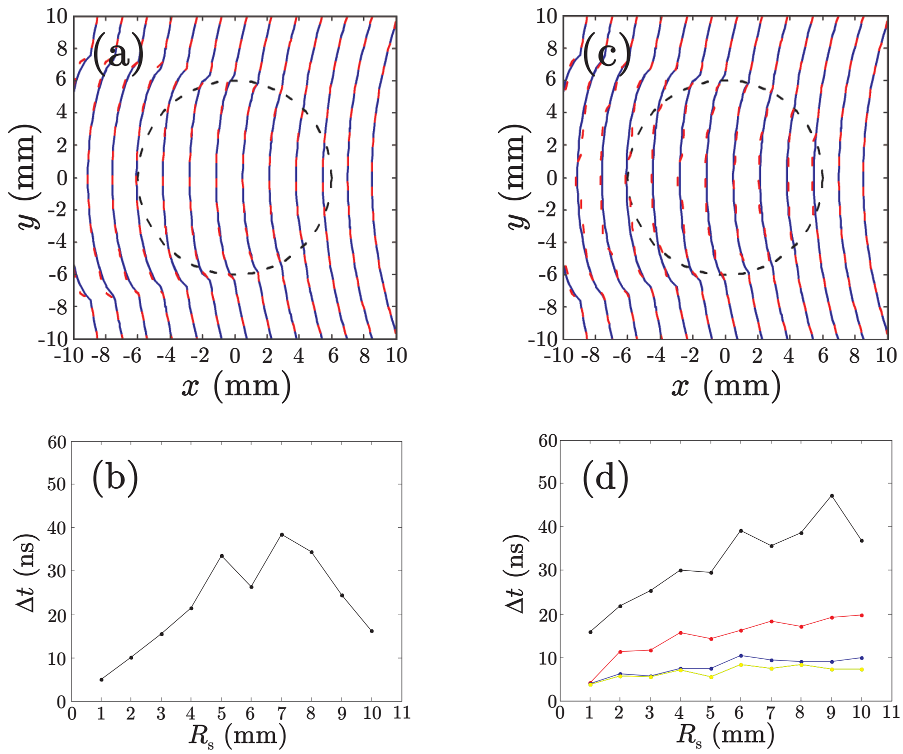

Figure 4. (Color online) Time-of-flight predicted by the straigth acoustic rays model and by considering also the refraction of the waves in the presence of a circular region with radius R_{s} and with a speed of sound $c_2 = 1650$ m/s. The background speed of sound is $c_1 = 1500$ m/s. The continuous blue curves in (a) and (c) represent points with a constant time-of-flight predicted with the straight acoustic rays model for $R_{\mathrm{s}} = 6$ mm. The equivalent curves obtained by considering the refraction of the waves and by considering a discrete approximation of the straight acoustic rays model are represented with dashed red lines in (a) and (c) respectively. (b) and (d) represent the root mean square difference of the time-of-flight predicted by the models in (a) and (c) as a function of R_{s}. The integration steps in (d) are $0.5\Delta xy$ (yellow), Δxy (green), $2\Delta xy$ (blue), $4\Delta xy$ (red) and $8\Delta xy$ (black).

4.3 Experimental results

The experimental results are shown in Fig. 5. In a first step, we made the reconstruction by considering a uniform speed of sound equal to the speed of sound in water at 20°C, namely $c_w = 1482$ m/s, and by taking the radius of the scanning circumference as $R = 39.15$ mm. Such parameters were calibrated by measuring an agar phantom with an optical absorbing area, for which the speed of sound mismatch is negligible. Then, the reconstructed images of the measuring phantoms obtained with the FBP algorithm by assuming a uniform speed of sound are displayed in Figs. 5a, 5b and 5c. The effect of the region with a different speed of sound is obvious as no representative images can be obtained if it is ignored. The boundary of the three phantoms can however be identified in Figs. 5a, 5b and 5c and is indicated with a dashed circumference. Then, in a second step, we considered a speed of sound c_p within the region limited by such circumferences and performed the reconstruction with the modification of the FBP algorithm described in section 2.2. The computation of the TOF was done with Eq. 9 by considering N points separated a distance equal to $2\Delta xy$, being Δxy the pixel size. The results obtained are shown in Figs. 5d, 5e and 5f. The value of c_p for each case is indicated in the caption of Fig. 5. It corresponds approximately to a 10% variation in the speed of sound with respect to water. The reconstructed images obtained show the validity of the model employed to make the correction in the case of having an *a priori* known non uniform speed of sound distribution.

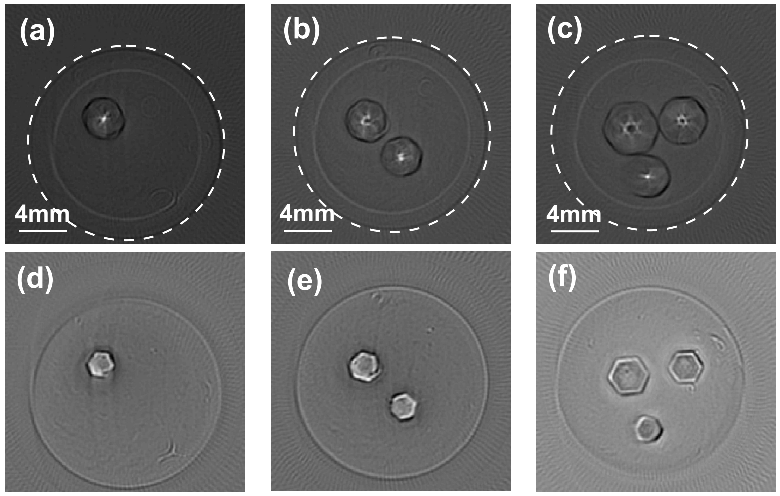

Figure 5. (a-c) Tomographic reconstructions obtained with the filtered back-projection algorithm for uniform acoustic media by considering a background speed of sound $c_w = 1482$ m/s and a scanning radius $R = 39.15$ mm. (d-f) Tomographic reconstructions obtained with the filtered back-projection algorithm by considering also a region with speed of sound c_p within the dashed circumferences indicated in (a-c). (d) $c_p = 1670$ m/s. (e) $c_p = 1670$ m/s. (f) $c_p = 1670$ m/s.

5. CONCLUSIONS

In this work, we have introduced a modification of the filtered back-projection algorithm for optoacoustic tomographic reconstructions in the case that an *a priori* known speed of sound distribution does exist. It relates to a modification of the curves along which the back-projection of the measured signals is done, so that each curve corresponds to a given value of the time-of-flight between the points of the curve and the position of the transducer. We have shown that the curves predicted by the straight acoustic rays model, in which the waves are assumed not to change direction as they propagate, are very similar to the curves predicted by considering also refraction effects in the case that the speed of sound variations are small, which applies in biological tissues. Then, the main effect the speed of sound variations is the time-sifting of the collected signals. The experimental results obtained with tissue-mimicking phantoms for which the speed of sound is approximately 10% higher than the speed of sound of water indicate the feasibility of correcting the reconstructed images in the presence of speed of sound heterogeneities.

APPENDIX A.

The angle θ_{AR} in Fig. 1 can be calculated as follows. When considering the SARM it is verified that

$$\overline{\mathrm{BD}'} = \overline{\mathrm{BD}} \tag{16}$$

where, according to the Snell's law, the segment $\overline{\mathrm{BD}}$ is given by

$$\overline{\mathrm{BD}} = \overline{\mathrm{BC}} \sin\theta_r \tag{17}$$

Then, the law of sines for the triangle CBD$'$ states that

$$\frac{\sin\theta_{AR}}{\overline{\mathrm{BD}'}} = \frac{\sin\left(\pi/2 + \theta_i - \theta_{AR}\right)}{\overline{\mathrm{BC}}} \tag{18}$$

By applying basic trigonometric transformations we obtain

$$\frac{\sin\theta_{AR}}{\overline{\mathrm{BD}'}} = \frac{\cos\theta_{AR}\cos\theta_i}{\overline{\mathrm{BC}}} + \frac{\sin\theta_{AR}\sin\theta_i}{\overline{\mathrm{BC}}} \tag{19}$$

Then, the rearrangment Eq. 19 by considering Eqs. 16 and 17 yields

$$\left(\frac{1}{\sin\theta_r} - \sin\theta_i\right)\tan\theta_{AR} = \cos\theta_i \tag{20}$$

Finally, by substituting Eq. 2 into Eq. 20 we have

$$\theta_{AR} = \arctan\left(\frac{c_2\sin\theta_i\cos\theta_i}{c_1 - c_2\sin^2\theta_i}\right) \tag{21}$$

ACKNOWLEDGMENTS

D.R. acknowledges support from the German Research Foundation (DFG) Research Grant (RA 1848/1) and the European Research Council (ERC) Starting Grant. V.N. acknowledges support from the ERC Advanced Investigator Award and the German Ministry of Education (BMBF) Innovation in Medicine Award.

REFERENCES

[1] Xu, M. and Wang, L. V., "Photoacoustic imaging in biomedicine," *Review of Scientific Instruments* **77**(4), 041101 (2006).

[2] Wang, X., Pang, Y., Ku, G., Xie, X., Stoica, G., and Wang, L. V., "Noninvasive laser-induced photoacoustic tomography for structural and functional *in vivo* imaging of the brain," *Nature Biotechnology* **21**(7), 803–806 (2003).

[3] Ntziachristos, V. and Razansky, D., "Molecular imaging by means of multispectral optoacoustic tomography (MSOT)," *Chemical Reviews* **110**(5), 2783–2794 (2010).

[4] Ntziachristos, V., "Going deeper than microscopy: the optical imaging frontier in biology," *Nature Methods* **7**(8), 603–614 (2010).

[5] Tam, A. C., "Applications of photo-acoustic sensing techniques," *Reviews of Modern Physics* **58**(2), 381–431 (1986).

[6] Wang, X., Xu, Y., Xu, M., Yokoo, S., Fry, E. S., and Wang, L. V., "Photoacoustic tomography of biological tissues with high cross-section resolution: Reconstruction and experiment," *Medical Physics* **29**(12), 2799–2805 (2002).

[7] Xu, M. and Wang, L. V., "Universal back-projection algorithm for photacoustic computed tomography," *Physical Review E* **71**(1), 016706 (2005).

[8] Xu, Y. and Wang, L. V., "Effects of acoustic heterogeneity in breast thermoacoustic tomography," *IEEE Transactions on Ultrasonics, Ferroelectrics and Frequency Control* **50**(9), 1134–1146 (2003).

[9] Jiang, H., Yuan, Z., and Gu, X., "Spatially varying optical and acoustic property reconstruction using finite-element-based photoacoustic tomography," *Journal of the Optical Society of America A* **23**(4), 878–888 (2006).

[10] Deán-Ben, X. L., Ma, R., Razansky, D., and Ntziachristos, V., "Statistical approach for optoacoustic image reconstruction in the presence of strong acoustic heterogeneities," *IEEE Transactions on Medical Imaging* **30**(2), 401–408 (2011).

[11] Deán-Ben, X. L., Ntziachristos, V., and Razansky, D., "Statistical optoacoustic image reconstruction using a-priori knowledge on the location of acoustic distortions," *Applied Physics Letters* (2011). DOI:10.1063/1.3564905.

[12] Szabo, T. L., [*Diagnostic Ultrasound Imaging: Inside Out*], Elsevier Academic Press, San Diego (USA) (2004).

[13] Kak, A. C. and Slaney, M., [*Principles of Computerized Tomographic Imaging*], IEEE Press, New York (USA) (2001).

[14] S Manohar, R G H Willemink, F. v. d. H. C. H. S. and van Leeuwen, T. G., "Concomitant speed-of-sound tomography in photoacoustic imaging," *Applied Physics Letters* **91**(13), 131911 (2007).

[15] Ma, R., Taruttis, A., Ntziachristos, V., and Razansky, D., "Multispectral optoacoustic tomography (MSOT) scanner for whole-body small animal imaging," *Optics Express* **17**(24), 21414–21426 (2009).